

Cite this: *Chem. Sci.*, 2026, 17, 7475

All publication charges for this article have been paid for by the Royal Society of Chemistry

Isolation of arylhalodiphosphenes: periodic trends in R–P=P–X bonding (X = Cl, Br, I)

John S. Wenger,¹ Nina Gaschik,² William J. Rowe,¹ Agamemnon E. Crumpton,¹ Bono van IJzendoorn¹ and Meera Mehta¹

For over a century, aryldiazonium halides have served as widely used building blocks within synthetic chemistry. They are vital intermediates in converting simple anilines to high-value products, including those needed to prepare pharmaceuticals, dyes, and functional materials. Despite the prevalence of these nitrogen-based organic salts in laboratories, structurally related phosphorus-based salts remain scarce. Herein, we report the isolation and structural characterization of a monomeric arylchlorodiphosphene, (M⁵FluInd*)P=P(Cl)(Et₂O)₂ (where M⁵FluInd* is a sterically demanding hydrindacene substituent), for the first time. The structure and reactivity of (M⁵FluInd*)P=P(Cl) were explored to compare the novel arylhalodiphosphene with compositionally related aryldiazonium chlorides, [RNN][Cl], and chloroiminophosphanes, RN=P(Cl). The P–P bond of (M⁵FluInd*)P=P(Cl) was cleaved *via* protonolysis to afford the parent phosphine, (M⁵FluInd*)PH₂. Halogen-exchange reactions between (M⁵FluInd*)P=P(Cl) and TMSX (TMS = trimethylsilyl, X = Br, I) afforded the related monomeric arylhalodiphosphenes, (M⁵FluInd*)P=P(X) (X = Br, I). Finally, the coordination complex, [(M⁵FluInd*)P=P(Cl)·Ag][CF₃SO₃], was isolated by treatment of (M⁵FluInd*)P=P(Cl) with AgCF₃SO₃. Periodic trends in the structure and bonding of (M⁵FluInd*)P=P(X) (X = Cl, Br, I) were investigated with spectroscopic, crystallographic, and computational methods. These studies confirm that the {PPX} moiety consists of a formal P–P double bond, and polar covalent P–X (X = Cl, Br, I) single bonds. (M⁵FluInd*)P=P(X) (X = Cl, Br, I) represent the first fully characterized, crystalline arylhalodiphosphenes and serve to advance the state of low-coordinate phosphorus chemistry.

Received 26th January 2026
Accepted 18th February 2026

DOI: 10.1039/d6sc00723f

rsc.li/chemical-science

Introduction

The isolation of heavy element analogues of common organic functional groups remains central to advancing our understanding of periodic trends and developing new precursors.^{1,2} The inherent challenges in stabilizing molecular species bearing multiple bonds between main-group elements heavier than those of the second period of the periodic table is encapsulated by the so-called “double bond rule”.^{3–5} Such molecules often form self-associated oligomers rather than retaining the heavy element–element multiple bond.⁶ Chemists may overcome this challenge by invoking thermodynamic stabilization whereby a Lewis acid and/or base is used to perturb the frontier molecular orbitals of the reactive unsaturated fragment,⁷ and/or *via* kinetic stabilization where the reactive fragment is sterically protected.^{8,9}

Initially reported in 1858, aryldiazonium chlorides are conveniently prepared by treatment of anilines with HCl and

NaNO₂ (Fig. 1).¹⁰ Aryldiazonium salts have served as important reagents and intermediates in numerous key named reactions, including the Sandmeyer reaction,¹¹ Pschorr reaction,¹² Gomberg–Bachmann reaction,¹³ Balz–Schiemann reaction,¹⁴ and Meerwein arylations.¹⁵ These reagents continue to be under intense investigation for their powerful utility in converting simple anilines to value-added products *via* diverse synthetic pathways.¹⁶ Despite the prevalence of diazonium salts across synthetic chemistry, analogous species in which one or both of the diazonium N atoms are replaced by a heavier pnictogen remains rare. In an early report, (Mes*)N=P(Cl) (Mes* = 2,4,6-*tert*-butylphenyl) was isolated by treating the corresponding aniline with an excess of PCl₃ and Et₃N (Fig. 1).¹⁷ (Mes*)N=P(Cl) may be viewed as a “monophosphadiazonium chloride” in which the Cl atom directly binds the terminal P atom, in contrast to diazonium chlorides which do not feature a similar N–Cl bond and instead exist as separated ion pairs even in the solid-state.¹⁸ Coordination of the Cl anion to the terminal P-atom disrupts multiple-bonding between the N and P atoms, and (Mes*)N=P(Cl) features an N–P double bond. (Mes*)N=P(Cl) may undergo halogen-exchange reactions to form (Mes*)N=P(X) (X = Br, I) by treating (Mes*)N=P(Cl) with the corresponding trimethylsilyl (TMS) halide (Fig. 1).

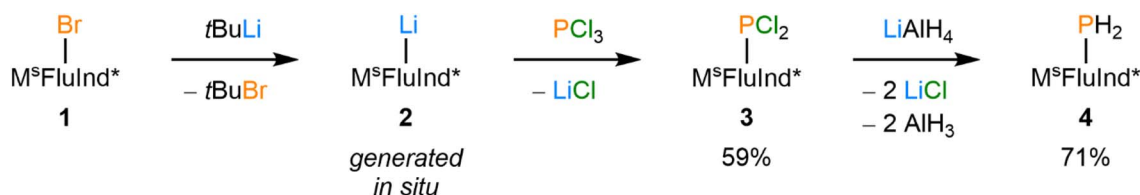
¹Department of Chemistry, University of Oxford, 12 Mansfield Road, Oxford, OX1 3QR, UK. E-mail: john.wenger@chem.ox.ac.uk; meera.mehta@chem.ox.ac.uk

²Department of Chemistry, Ludwig-Maximilians-Universität München, Butenandtstrasse 5-13, 81377 München, Germany





Fig. 1 General synthesis of [RNN][Cl] (i = excess HCl, excess NaNO₂). Synthesis of (Mes*)NPCl and [ClP(μ-PMes*)]₂ (ii = excess PCl₃, excess Et₃N). Synthesis of [(Mes*)NP][AlCl₄] (iii = AlCl₃). Synthesis of (Mes*)NPX (iv = TMSX; X = Br, I). Depiction of (M^sFluInd*)PPX (X = Cl, Br, I) reported herein. Structural diagrams of ligands M^sFluInd* and Mes*.



Scheme 1 Synthesis of compounds 2, 3, and 4.

(Mes*)N=P(Cl) has served as a seminal precursor to phosphadiazonium compounds. For example, treatment of (Mes*)N=P(Cl) with AlCl₃ resulted in chloride abstraction to form the iminophosphenium tetrachloroaluminate, [(Mes*)NP][AlCl₄] (Fig. 1). The same group later isolated a range of oxy-substituted iminophosphanes by treatment of (Mes*)N=P(Cl) with silver or lithium salts.¹⁹ Further, iminophosphenium species may also be generated *in situ* by reacting with GaCl₃.²⁰ Recently, the chloroiminophosphane, (Ter*)N=P(Cl) [Ter* = bis(*ortho-m*-hexaisopropylterphenyl)phenyl] was prepared from the bulky aniline (Ter*)NH₂ and employed as a precursor in the isolation of a two-coordinate phosphindene oxide, (Ter*)NBnPO.²¹ Further, (M^sFluInd*)N=P(Cl) was recently prepared from (M^sFluInd*)NH₂ and served as a precursor for an aryliminophosphinyl radical, (M^sFluInd*)NP.²²

Numerous diphosphenes of the form RP=PR' have been reported since the seminal discovery of the diaryldiphosphene, (Mes*)P=P(Mes*).²³ The stability of diphosphenes is largely attributed to the presence of bulky substituents at each P atom that form a sterically protected cavity for the P-P double-bonded core to reside.²⁴ Compounds featuring {P₂} fragments stabilized by either carbene ligands or transition metals have also been isolated.^{25–30}

Asymmetric diphosphenes that feature an alkyl, alkoxy, or amino group in addition to an aryl substituent have also been reported and, in some cases, have served as precursors to donor-stabilized diphosphadiazonium species.^{31–34} Treatment of the aminoaryldiphosphenes, (Mes*)P=P(NR₂) (NR₂ = N(^tPr)₂, N(cyclohexyl)₂, or 2,2,6,6-tetramethylpiperidine) with one equivalent of HCF₃SO₃ affords ammonium salts, [(Mes*)P=P(NHR₂)]⁺[CF₃SO₃]⁻, which are stable in solution at –50 °C.³⁵ Remarkably, treatment of a 1 : 1 mixture of (Mes*)P=P(NR₂) and Ph₃P with two equivalents of HCF₃SO₃ affords [(Mes*)P=P(PPh₃)]⁺[CF₃SO₃]⁻, which was initially reported as a donor-stabilized diphosphadiazonium cation. However, crystallographic and computational data indicate that [(Mes*)P=P(PPh₃)]⁺[CF₃SO₃]⁻ is best described as a diphosphene with an adjacent triphenylphosphonium center.³⁶

Treatment of (Mes*)P=P(N^tPr)₂ with HCl was reported to form monomeric (Mes*)P=P(Cl) *via* the loss of HN^tPr₂.³⁷ However, (Mes*)P=P(Cl) was reported to exist only transiently at –50 °C in solution, and its structure has only been inferred by ³¹P NMR analysis and follow-on reactivity studies with organolithium reagents to form asymmetric diphosphenes.³⁸ Monomeric (Mes*)P=P(X) (X = Br, I) were reported to be prepared by treatment of (Mes*)P=P(N^tPr)₂ with HX (X = Br, I), or by treatment of [(Mes*)P=P(PPh₃)]⁺[CF₃SO₃]⁻ with [Et₃NH][X] (X = Br, I)



at $-78\text{ }^{\circ}\text{C}$, but again these compounds were only characterized by ^{31}P NMR spectroscopy and it is unclear at which temperature these spectra were collected.^{35,39} The existence of monomeric $(\text{Mes}^*)\text{P}=\text{PX}$ ($\text{X} = \text{Cl}, \text{Br}, \text{I}$) as isolable reagents has recently been called into question in the absence of conclusive analytical evidence and crystallographic characterization; treatment of the primary phosphine, $(\text{Mes}^*)\text{PH}_2$ with an excess of PCl_3 and NEt_3 , does not afford monomeric $(\text{Mes}^*)\text{P}=\text{PCl}$, but rather affords the dimeric form $[\text{ClP}(\mu\text{-PMes}^*)]_2$, which was characterized in both solution and solid-state (Fig. 1).^{36,40,41}

Herein, we report the isolation of a crystalline, monomeric arylchlorodiphosphene, $(\text{M}^{\text{s}}\text{FluInd}^*)\text{P}=\text{PCl}$ (**8**) (Fig. 1). Spectroscopic, crystallographic, and computational characterization of compound **8** confirms the presence of a formal P–P double bond and a polar, covalent P–Cl single bond, in contrast to compositionally analogous aryldiazonium chlorides of the form $[\text{RNN}][\text{Cl}]$. The terminal $\{\text{PPCl}\}$ unit in **8** is kinetically stabilized by the sterically demanding hydrindacene substituent, $\text{M}^{\text{s}}\text{FluInd}^*$.⁴² The unsaturated P–P bond in **8** may be cleaved *via* protonolysis to form the primary phosphine, $(\text{M}^{\text{s}}\text{FluInd}^*)\text{PH}_2$ (**4**). Treatment of compound **8** with TMSBr or TMSI affords $(\text{M}^{\text{s}}\text{FluInd}^*)\text{PPBr}$ (**9**), and $(\text{M}^{\text{s}}\text{FluInd}^*)\text{PPI}$ (**10**), respectively, highlighting the synthetic

utility of the terminal P–Cl bond in **8**. Attempts to abstract the Cl atom from **8** with AlCl_3 or GaCl_3 afforded complex reaction mixtures, while treatment of **8** with AgCF_3SO_3 afforded the coordination complex, $[(\text{M}^{\text{s}}\text{FluInd}^*)\text{PPCl}\cdot\text{Ag}][\text{CF}_3\text{SO}_3]$ (**11**). Periodic trends in structure and bonding between the novel catalogue of isolable arylhalodiphosphenes **8**, **9**, and **10** were explored with spectroscopic, crystallographic, and computational methods.

Results and discussion

Synthesis of novel phosphine precursors

Inspired by the success of bulky hydrindacene-based ligands in stabilizing reactive molecular fragments,^{22,42–59} literature known $(\text{M}^{\text{s}}\text{FluInd}^*)\text{Br}$ (**1**) was treated with an excess of *tert*-butyl lithium to form $(\text{M}^{\text{s}}\text{FluInd}^*)\text{Li}$ (**2**) *in situ*,⁴² which was subsequently treated with PCl_3 to afford $(\text{M}^{\text{s}}\text{FluInd}^*)\text{PCl}_2$ (**3**), characterized as the hexane solvate (Scheme 1). Compound **3** was then reduced with an excess of LiAlH_4 to afford $(\text{M}^{\text{s}}\text{FluInd}^*)\text{PH}_2$ (**4**) (Scheme 1). However, we found it was most efficient to synthesize **4** directly from **1** without fully isolating **3**. Like other primary phosphines bearing bulky aryl substituents, **4** is air-stable in both the solid-state and in solution.^{60,61} Compound **4**



Fig. 2 Thermal ellipsoid plot (50% probability) of (A) **4** · (hexane), (B) **5** · (toluene)_{2.5}, (C) **6** · (Et₂O)₂, and (D) **7** · (Et₂O)₂. Solvent molecules, C-bound H atoms, and disordered components are omitted for clarity. Only the major component of disorder is displayed in all cases. Select C atoms and H atoms are shown as spheres of arbitrary radius for clarity. Color code: P orange, Cl dark green, Si dark yellow, K sky blue, C black, H grey.



could be crystallized from a $-30\text{ }^{\circ}\text{C}$ solution of hexane to afford colorless blocks of $4\cdot(\text{hexane})$. Structural characterization of $4\cdot(\text{hexane})$ by single-crystal X-ray diffraction (SC-XRD) confirms the presence of a terminal $\{\text{PH}_2\}$ group within the sterically protected environment created by the flanking fluorenyl substituents of the $\text{M}^{\text{s}}\text{FluInd}^*$ ligand (Fig. 2A).

Compound $4\cdot(\text{hexane})$ was reacted with potassium benzylate (KBz) in benzene to form intensely red solutions of $(\text{M}^{\text{s}}\text{FluInd}^*)\text{PHK}$ (**5**) *in situ* (Scheme 2), which was structurally characterized as a toluene solvate (Fig. 2B). In the solid-state, $5\cdot(\text{toluene})_{2.5}$ exists as a centrosymmetric dimer in which a disordered toluene molecule resides on the crystallographic inversion center and coordinates the potassium ions. Each potassium ion is further coordinated by a 6-membered ring within the fluorenyl groups and by the anionic P-donor.

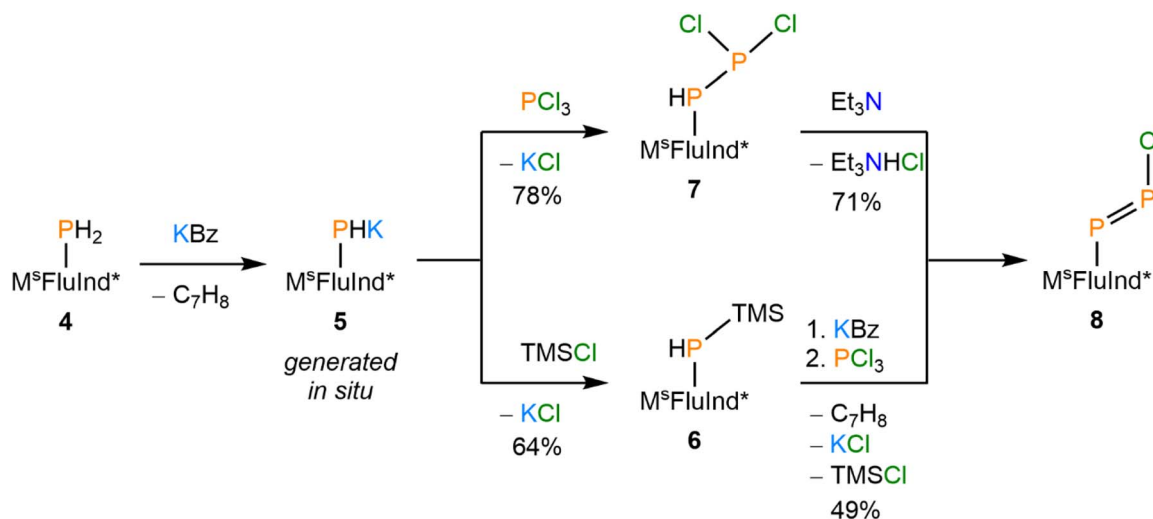
We hypothesized that a silylated phosphine substituted with the sterically demanding $\text{M}^{\text{s}}\text{FluInd}^*$ substituent could serve as an effective precursor for the synthesis of unsaturated main-group species. $(\text{M}^{\text{s}}\text{FluInd}^*)\text{PTMSH}$ (**6**) was isolated *via* sequential treatment of $4\cdot(\text{hexane})$ with KBz followed by TMSCl (Scheme 2). Colorless blocks of analytically pure $6\cdot(\text{Et}_2\text{O})_2$ were isolated by crystallization from Et_2O solutions at $-30\text{ }^{\circ}\text{C}$. $6\cdot(\text{Et}_2\text{O})_2$ crystallizes in the $P4_21m$ space-group on a special position distinguished by a two-fold rotation axis and two mirror planes, such that 0.25 of the $\text{M}^{\text{s}}\text{FluInd}^*$ ligand resides in the asymmetric unit and the central $\{\text{PTMSH}\}$ unit is disordered about these symmetry elements (Fig. 2C).

Sequential treatment of $4\cdot(\text{hexane})$ with KBz followed by PCl_3 successfully afforded $(\text{M}^{\text{s}}\text{FluInd}^*)\text{PHPCl}_2$ (**7**) which was obtained as the Et_2O disolvate from solutions of **7** in Et_2O at $-30\text{ }^{\circ}\text{C}$ (Scheme 2). The $^{31}\text{P}\{^1\text{H}\}$ nuclear magnetic resonance (NMR) spectrum of $7\cdot(\text{Et}_2\text{O})_2$ exhibits a prominent pair of doublets at -41 ppm and 209 ppm with a $^1J_{\text{PP}}$ value of 247 Hz , consistent with the presence of a P–P single bond in **7**.⁶² Additionally, the ^{31}P and ^1H NMR spectra confirm a P-bound proton in **7** with $^1J_{\text{PH}} = 219\text{ Hz}$ and $^2J_{\text{PH}} = 14.5\text{ Hz}$. Crystals of $7\cdot(\text{Et}_2\text{O})_2$ are crystallographically isomorphic with $6\cdot(\text{Et}_2\text{O})_2$ and feature

a terminal $\{\text{PHPCl}_2\}$ motif disordered about multiple positions (Fig. 2D). Unfortunately, we were unable to isolate $7\cdot(\text{Et}_2\text{O})_2$ as an analytically pure material; we attribute our inability to purify **7** to the high crystallinity and similar solubility of $\text{M}^{\text{s}}\text{FluInd}^*$ -containing impurities, a common challenge associated with the use of such sterically demanding substituents.^{21,42,63}



Fig. 3 Stacked (A) ^{31}P NMR spectra and (B) IR spectra of $8\cdot(\text{Et}_2\text{O})_2$, $9\cdot(\text{Et}_2\text{O})_2$, and $10\cdot(\text{Et}_2\text{O})_2$. Signals in the IR spectrum assigned to a P–X bond stretching mode are denoted with an asterisk.



Scheme 2 Synthesis of compounds **5**, **6**, **7**, and **8**.



Synthesis and reactivity of a monomeric arylchlorodiphosphene

Treatment of a hexane solution of $7 \cdot (\text{Et}_2\text{O})_2$ with triethylamine resulted in the formation of a yellow suspension (Scheme 2). Removal of the solid by-product $[\text{Et}_3\text{NH}][\text{Cl}]$ and volatiles, followed by recrystallization of the residue from Et_2O resulted in the isolation of yellow crystals. Analysis of the crystalline product by ^{31}P NMR spectroscopy revealed two new doublets in the spectrum, which do not exhibit any ^1H coupling (Fig. 3A). The ^{31}P NMR resonances of the product are shifted strongly downfield with respect to the precursor at 433 ppm and 502 ppm and exhibit a larger $^1J_{\text{PP}}$ coupling constant of 574 Hz, consistent with an asymmetric diphosphene species with a P–P double bond.^{31,36,64–66} Furthermore, the infrared (IR) spectrum of the product features a strong band assigned to the P–Cl stretch that appears at a lower wavenumber ($\nu_{\text{P-Cl}} = 451 \text{ cm}^{-1}$) relative to that of $7 \cdot (\text{Et}_2\text{O})_2$ ($\nu_{\text{P-Cl}} = 461 \text{ cm}^{-1}$) (Fig. 3B, SI Fig. S34).

Analysis of the yellow crystals by SC-XRD reveals the sample to be crystallographically isomorphous with those of $6 \cdot (\text{Et}_2\text{O})_2$ and $7 \cdot (\text{Et}_2\text{O})_2$; the product also crystallizes in the $P\bar{4}2_1m$ space

group with nearly identical unit cell parameters. However, solution of the solid-state structure confirms a distinct Fourier difference map within the cavity created by the $\text{M}^{\text{s}}\text{FluInd}^*$ ligand. Indeed, the crystallographic data are fit excellently by $8 \cdot (\text{Et}_2\text{O})_2$ ($R_1 = 4.62\%$). Our model features disorder between a major *E*-isomer with an occupancy of 85% (Fig. 4A) and a minor *Z*-isomer with an occupancy of 15% with respect to the asymmetric diphosphene unit. The major *E*-isomer is further disordered about two positions, and the entire $\{\text{PPCl}\}$ motif is disordered about a special position. We note that the connectivity of $8 \cdot (\text{Et}_2\text{O})_2$ is unambiguous, but meaningful discussion of structural parameters is precluded by this disorder. Remarkably, compound **8** may also be synthesized by treatment of $6 \cdot (\text{Et}_2\text{O})_2$ with KBz followed by PCl_3 *via* the formal elimination of KCl and TMSCl (Scheme 2).

For most monomeric diphosphenes, the synthesis of *Z*-isomers from *E*-isomers requires photolytic conditions and low temperatures, and warming solutions of the resulting *Z*-isomer to room-temperature results in the formation of the more stable *E*-isomer.^{31,67,68} The observed isomerism in the solid-state structure may be the result of a photoisomerization reaction

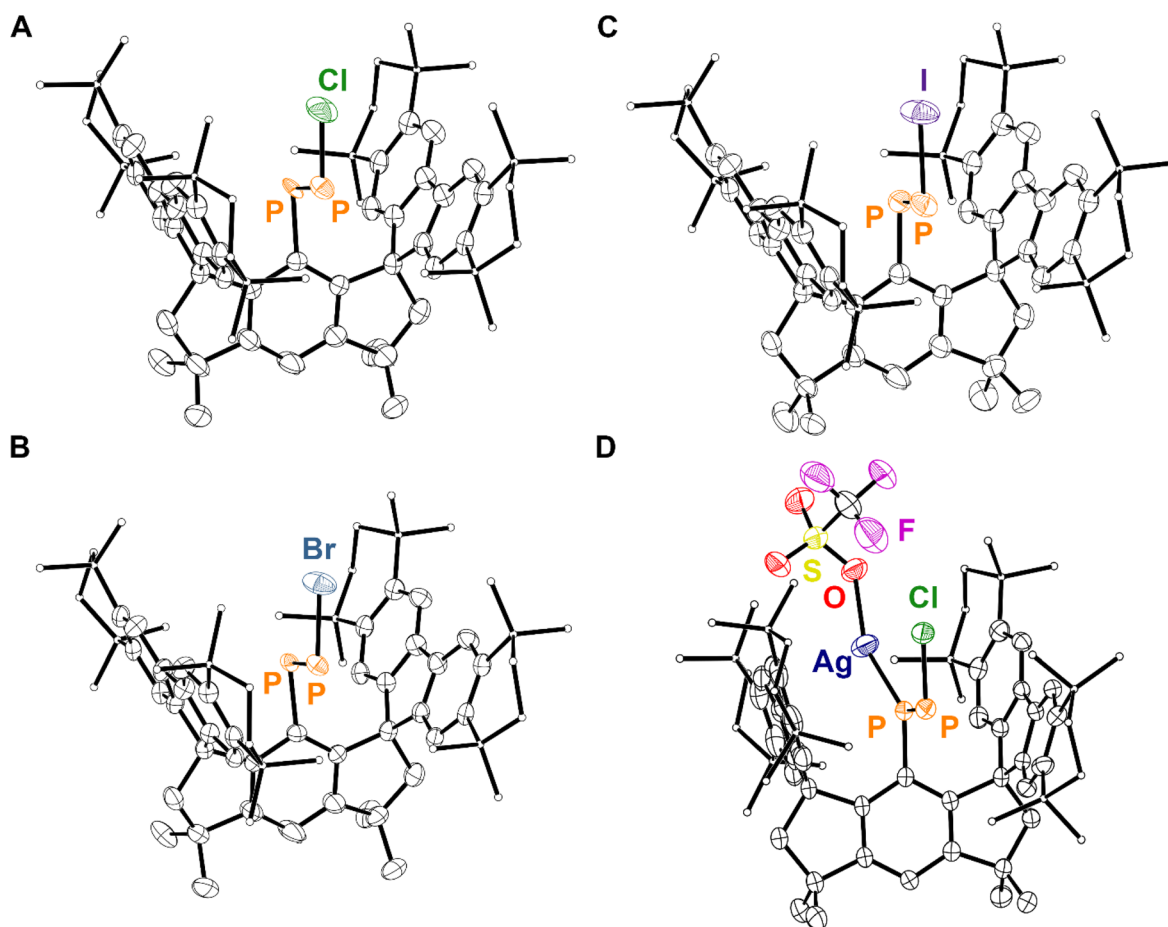


Fig. 4 Thermal ellipsoid plots (50% probability) depicting the major *E*-isomer for (A) $8 \cdot (\text{Et}_2\text{O})_2$, (B) $9 \cdot (\text{Et}_2\text{O})_2$, (C) $10 \cdot (\text{Et}_2\text{O})_2$, and (D) **11**. The refined *E* : *Z* occupancy ratios in our models are 85 : 15, 78 : 22, 60 : 40, and 67 : 33 for $8 \cdot (\text{Et}_2\text{O})_2$, $9 \cdot (\text{Et}_2\text{O})_2$, $10 \cdot (\text{Et}_2\text{O})_2$, and **11**, respectively. Only the major component of disorder for the *E*-isomer of $8 \cdot (\text{Et}_2\text{O})_2$ and $9 \cdot (\text{Et}_2\text{O})_2$ are depicted. Solvent molecules, H atoms, and disordered components are omitted for clarity. Select C atoms are shown as spheres of arbitrary radius for clarity. Color code: P orange, Cl dark green, Br blue, I purple, Ag navy, F pink, S yellow, O red, C black.



to Ag^+ (Fig. 4D).³¹ Remarkably, the solid-state structure of **11** features a two-component disorder arising from the presence of the *E* and the *Z* isomer of the coordinated diphosphene, **8**, in a 68 : 32 occupancy ratio, respectively. These results ultimately highlight the divergent reactivity between the chloroiminophosphane, $(\text{Mes}^*)\text{N}=\text{P}(\text{Cl})$, and compound **8**.

Theoretical analysis of monomeric arylhalodiphosphenes

Curious to investigate periodic trends in structure and bonding amongst this newly discovered class of monomeric arylhalodiphosphenes, the theoretical molecules *E*-**8***, *E*-**9***, *E*-**10***, *Z*-**8***, *Z*-**9***, and *Z*-**10*** (pictured in the SI Fig. S73–S75) were optimized at the PBE0-D3/def2-TZVPP level of theory. Selected bond metrics are provided in SI Tables S5 and S6.

Frequency calculations predict the enthalpy of formation of *E*-**8*** to be 2.96 kcal mol⁻¹ more favorable than that of *Z*-**8***. Similarly, *E*-**9*** and *E*-**10*** are predicted to be more stable than *Z*-**9*** and *Z*-**10*** by 3.48 kcal mol⁻¹ and 3.83 kcal mol⁻¹, respectively. Calculated gas-phase ³¹P NMR spectroscopic data (PBE0-D4/pcseg-2//PBE0-D3/def2-TZVPP) found the ¹*J*_{PP} coupling

constant for *E*-**8*** to be more consistent with our experimental value than that calculated for *Z*-**8*** (SI Table S21). Subsequent discussions are limited to the more stable theoretical *E*-isomers. The P–X bond stretching frequencies for *E*-**8***, *E*-**9***, and *E*-**10*** were calculated to be 481, 392, and 357 cm⁻¹. The associated P–X stretching force constants are 2.10, 1.73, and 1.45 mdyne/Å, respectively, showing the weakening of the P–X bond from *E*-**8*** > *E*-**9*** > *E*-**10***. The P–P bond stretching frequencies for *E*-**8***, *E*-**9***, and *E*-**10*** are 656, 653, and 649 cm⁻¹ and predicted to have negligible intensity.

A single point energy calculation at the DKH-PBE0/old-DKH-TZVPP level of theory was performed on the optimized coordinates of *E*-**8***, *E*-**9***, and *E*-**10*** for a detailed computational analysis (SI Tables S10–S17), and the summarized results are discussed. Topological analysis of the electron density (ρ)⁷³ of *E*-**8***, *E*-**9***, and *E*-**10*** along the P–P interatomic vector reveals bond critical points, at which $\rho = 0.156$, 0.155, and 0.154 e⁻ Bohr⁻³, respectively (Fig. 5A). The negative Laplacian of ρ ($\nabla^2\rho$) in the P–P valence region signifies significant charge concentration and covalency of the dipnictene bond of *E*-**8***, *E*-**9***, and *E*-**10*** (Fig. 5B).⁷⁴ We also calculate significant ellipticity of ρ (ϵ)

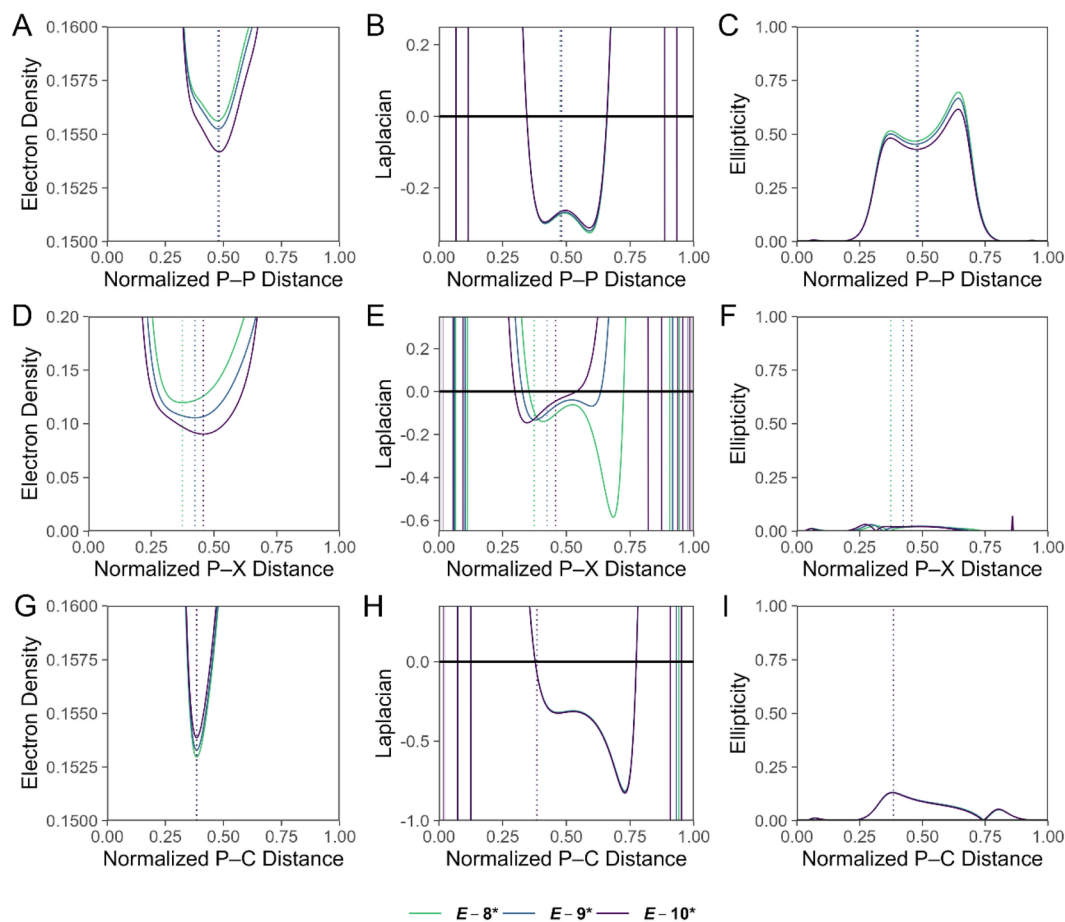


Fig. 5 Values of (A) ρ (e⁻ Bohr⁻³), (B) $\nabla^2\rho$ (e⁻ Bohr⁻⁵), and (C) ϵ for *E*-**8***, *E*-**9***, and *E*-**10*** along the P–P interatomic vector, with the C-bound P atom at 0.00 and the X-bound P atom (X = Cl, Br, I) at 1.00 along the horizontal axis. Values of (D) ρ (e⁻ Bohr⁻³), (E) $\nabla^2\rho$ (e⁻ Bohr⁻⁵), and (F) ϵ for *E*-**8***, *E*-**9***, and *E*-**10*** along the P–X (X = Cl, Br, I) interatomic vector. Values of (G) ρ (e⁻ Bohr⁻³), (H) $\nabla^2\rho$ (e⁻ Bohr⁻⁵), and (I) ϵ for *E*-**8***, *E*-**9***, and *E*-**10*** along the P–C interatomic vector. The bond lengths are normalized to 1.00. The location of the (3, -1) critical point is shown with a dashed vertical line. Calculations were performed at the (DKH-PBE0/old-DKH-TZVPP//PBE0-D3/TZVPP) level of theory.



in the P–P valence region, consistent with formal double bond character of the interaction (Fig. 5C). Along the P–X (X = Cl, Br, I) interatomic vector, $\rho = 0.120, 0.106,$ and $0.090 \text{ e}^- \text{ Bohr}^{-3}$ at the bond critical point for *E-8**, *E-9**, and *E-10**, respectively, reflecting the weakening of the P–X bond from *E-8** > *E-9** > *E-10** (Fig. 5D). The $\nabla^2\rho$ function in the P–Cl bonding region in *E-8** is highly asymmetric and signifies a polarization of charge towards the more electronegative Cl atom, reflecting the ionic character of the bond (Fig. 5E). For *E-9** and *E-10**, the $\nabla^2\rho$ function in the P–X (Br, I) bonding region is dramatically less polarized (Fig. 5E). Topological analysis along the P–C bond path in *E-8**, *E-9**, and *E-10** is reminiscent of that of the P–Cl bond in *E-8**, but features higher values of ρ at the bond critical point, and values of the $\nabla^2\rho$ function in the bonding region are less polarized and more negative, consistent with a stronger, more covalent bonding interaction (Fig. 5G and H). Values for ϵ along the P–X (X = Cl, Br, I) and P–C bond paths in *E-8**, *E-9**, and *E-10** are low, but not negligible and likely signify π -type donor–acceptor interactions (Fig. 5F and I).

The highest occupied molecular orbital (HOMO) of *E-8** is highly delocalized and largely comprised of contribution by the P–P π bond and a Cl-centered lone pair (Fig. 6A). The lowest unoccupied molecular orbital (LUMO) of *E-8** is largely defined

by P–P π^* contribution and the LUMO+2 of *E-8** is largely defined by P–Cl σ^* contribution (Fig. 6B and C). Similar results were obtained for *E-9** and *E-10**; however, the LUMO+1 is largely comprised of the P–X σ^* (X = Br, I) contribution in these cases (SI Fig. S77–S82).

Energetic analysis of the canonical molecular orbitals (CMO) reveals the HOMO increases in energy from *E-8** < *E-9** < *E-10** while the LUMO and LUMO+1 decrease in energy from *E-8** > *E-9** > *E-10** (Fig. 7). These data are consistent with the weakening of the P–P and P–X (X = Cl, Br, I) bonds as the terminal halide becomes heavier. We performed a similar energetic analysis of the simple, theoretical diaryldiphosphene, *E*-MesP=PMe₂ (*E-12**), for comparison, and *E-12** features a significantly lower LUMO than the theoretical arylhalodiphosphenes (Fig. 7).

Experimental ultraviolet-visible (UV-Vis) spectra of **8**·(Et₂O)₂, **9**·(Et₂O)₂, and **10**·(Et₂O)₂ feature λ_{max} values of 349 nm, 355 nm, and 370 nm, respectively, reflecting the lowering of the LUMO from *E-8** > *E-9** > *E-10**. Time-dependent density functional theory (TD-DFT) calculations suggest that the observed yellow color in these species is predicted to arise from electronic transitions between the HOMO–3/HOMO–2/HOMO–1/HOMO and the LUMO in each case (SI Tables S12–S14).



Fig. 6 (A) HOMO, (B) LUMO, and (C) LUMO+2 of *E-8** (isovalue = 0.015). Surface plots (isovalue = 0.06) for *E-8**, depicting the (D) P–P π bonding NLMO, (E) P–P π^* antibonding NLMO, (F) P–Cl σ^* antibonding NLMO, (G) a Cl-centered lone pair, (H) overlap between a Cl-centered lone pair and the P–P π^* antibonding NLMO, and (I) overlap between the P–C σ bonding NLMO and the P–Cl σ^* antibonding NLMO. In Fig. 6A–H, the molecule is viewed down the plane defined by the {PPCl} unit. In Fig. 6I, the molecule is oriented differently for clarity of the displayed NLMOs. Color code: P orange, Cl dark green, C black, H grey. Displayed NLMOs are pre-orthogonalized. Calculations were performed at the (DKH-PBE0/old-DKH-TZVPP//PBE0-D3/TZVPP) level of theory.



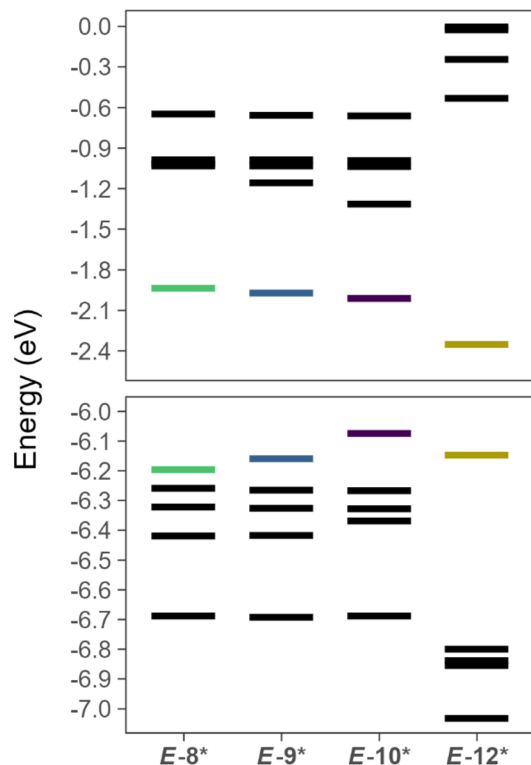


Fig. 7 Calculated orbital energies (DKH-PBE0/old-DKH-TZVPP//PBE0/def2-TZVPP) for *E-8**, *E-9**, *E-10**, and *E-12** with frontier molecular orbitals shown in color. The upper panel contains the values for the LUMO, LUMO+1, LUMO+2, LUMO+3, and LUMO+4. The lower panel contains values for the HOMO, HOMO-1, HOMO-2, HOMO-3, and HOMO-4.

Natural Population Analysis (NPA) reveals a systematic decrease in negative charge on the halide from *E-8** > *E-9** > *E-10** (SI Fig. S84). Similarly, a decrease in positive charge is calculated for the X-bound P atom from *E-8** > *E-9** > *E-10**. These results are consistent with a less polarized P-X bond as the halide increases in size. The theoretical asymmetric diphosphenes, *E-MesP=P*(^tBu) (*E-13**), *E-MesP=P*(SiMe₃) (*E-14**), *E-MesP=P*(OMe) (*E-15**), *E-MesP=P*(NMe₂) (*E-16**), [*E-MesP=P*(NMe₃)]⁺ (*E-17**), and [*E-MesP=P*(PMe₃)]⁺ (*E-18**) were investigated at the same level of theory to compare polarization of the P-P bond in arylhalodiphosphenes with other asymmetric diphosphenes (pictured in the SI Fig. S83). NPA analysis suggests that among the arylhalodiphosphenes, the P-P bond becomes increasingly polarized from *E-8** < *E-9** < *E-10**, as the positive charge on the X-bound (X = Cl, Br, I) P atom decreases. The alkyl-substituted diphosphene, *E-13** features a relatively unpolarized P-P bond, similar to *E-8** and *E-9**. However, the heteroatom-substituted aryldiphosphenes feature relatively large polarization of the P-P bond, which is more akin to *E-10**, with the exception of the ammonium cation, *E-17**.

Natural Localized Molecular Orbital (NLMO) analysis of *E-8** reveals the presence of a P-P π NLMO and a P-P π* NLMO, which closely resemble the nodal structure calculated for the HOMO and LUMO, respectively (Fig. 6D and E). The NLMO analysis further identified a P-Cl σ* NLMO which resembles the

LUMO+2 and a filled Cl-centered 3p orbital, which appears prominently in both the HOMO and LUMO (Fig. 6F and G).

Intriguingly, second-order perturbation theory analysis of *E-8**, *E-9**, and *E-10** reveals delocalization from an X-centered (X = Cl, Br, I) lone pair to the P-P π* orbital to afford an energy of stabilization of 9.39, 7.82, and 6.30 kcal mol⁻¹, respectively (Fig. 6H). Furthermore, delocalization of electron density from the P-C σ orbital and the lone pair of the C-bound P atom to the terminal P-X σ* orbital (X = Cl, Br, I) afford a total energy of stabilization of 4.73, 4.92, and 4.53 kcal mol⁻¹ for *E-8**, *E-9**, and *E-10**, respectively (Fig. 6I). In order to more broadly assess the relative strengths of the non-covalent donor-acceptor interactions present in *E-8**, *E-9**, and *E-10**, we performed deletion calculations, in which all non-covalent interactions from the halide to the {P₂} unit and *vice versa* were deleted. The removal of these non-covalent interactions resulted in the destabilization of *E-8**, *E-9**, and *E-10** by 30.73, 25.73, and 19.96 kcal mol⁻¹, respectively. The results of these deletion calculations are in line with the general trend that non-covalent interactions between the halide and the {P₂} unit become less efficient from *E-8** > *E-9** > *E-10**.

Natural Resonance Theory (NRT) analysis identified leading resonance structures featuring a P-P double bond and a polar, covalent P-X (X = Cl, Br, I) single bond for the simple theoretical molecules *E-MePPCl*, *E-MePPBr*, and *E-MePPI*, respectively (SI Tables S18-S20). The NRT analysis is consistent with increasing ionicity of the P-X bond from *E-MePPI* < *E-MePPBr* < *E-MePPCl*.

Conclusions

In conclusion, we report the isolation of **8**·(Et₂O)₂, a thermally robust, monomeric arylhalodiphosphene. Compound **8** features a terminal {PPCl} unit and can thus be regarded as a 'masked' aryldiphosphadiazonium chloride, marking a significant advancement in the context of decades of diphosphene chemistry. The P-P bond of **8** could be cleaved *via* protonolysis by aqueous hydrobromic acid, and the synthetic utility of the P-Cl bond in **8** was demonstrated in halogen-exchange reactions with TMSBr and TMSI to form the monomeric arylhalodiphosphenes, **9** and **10**, respectively. Treatment of **8** with GaCl₃ or AlCl₃ resulted in rapid decomposition to form complex reaction mixtures. However, **8** participates in coordination chemistry that is typical of diphosphenes; treatment of **8** with AgCF₃SO₃ forms, **11**. In **8**, **9**, **10**, and **11**, SC-XRD experiments clearly identified the presence of both the *E* and the *Z* isomer with respect to the diphosphene motif in solid state. Our theoretical investigation elucidated trends in bonding amongst the theoretical arylhalodiphosphenes *E-8**, *E-9**, and *E-10**. Notably, the HOMO increases in energy, the LUMO and LUMO+1 decrease in energy, and the P-X (X = Cl, Br, I) bond weakens as the terminal halide increases in size. Further investigations into the reactivity of monomeric arylhalodiphosphenes are currently underway, as are efforts to isolate a genuine diphosphadiazonium salt.

Author contributions

J. S. W.: conceptualization, data curation, funding acquisition, investigation (chemical synthesis, data acquisition, X-ray



crystallography, DFT methods), methodology, visualization, writing – original draft, writing – review and editing. N. G.: investigation (chemical synthesis). W. J. R.: investigation (chemical synthesis). A. E. C.: investigation (X-ray crystallography). B. v. I.: investigation (acquisition of VT-NMR data). M. M.: conceptualization, funding acquisition, project administration, resources, supervision, writing – review and editing.

Conflicts of interest

There are no conflicts to declare.

Data availability

CCDC 2501235–2501241, 2512823, 2512824, and 2523752 contain the supplementary crystallographic data for this paper.^{75a–j}

The data supporting this article have been included as part of the supplementary information (SI). Supplementary information is available. See DOI: <https://doi.org/10.1039/d6sc00723f>.

Acknowledgements

We thank the University of Oxford and UKRI for funding (EP/Y037391/1) and supporting M. M. We also thank the ERC for funding a Marie Skłodowska-Curie Fellowship (101205172) and supporting J. S. W. We are also grateful to the University of Oxford for computing resources.

Notes and references

- R. C. Fischer and P. P. Power, *Chem. Rev.*, 2010, **110**(7), 3877–3923.
- D. You and F. P. Gabbaï, *Trends Chem.*, 2019, **1**(5), 485–496.
- L. Zhao, S. Pan, N. Holzmann, P. Schwerdtfeger and G. Frenking, *Chem. Rev.*, 2019, **119**(14), 8781–8845.
- R. West, *Angew. Chem., Int. Ed.*, 1987, **26**(12), 1201–1211.
- L. E. Gusel'nikov and N. S. Nametkin, *Chem. Rev.*, 1979, **79**(6), 529–577.
- V. J. Eilrich and E. Hey-Hawkins, *Coord. Chem. Rev.*, 2021, **437**, 213749.
- V. Nesterov, D. Reiter, P. Bag, P. Frisch, R. Holzner, A. Porzelt and S. Inoue, *Chem. Rev.*, 2018, **118**(19), 9678–9842.
- E. Rivard and P. P. Power, *Inorg. Chem.*, 2007, **46**(24), 10047–10064.
- J. S. Wenger and T. C. Johnstone, *Dalton Trans.*, 2024, **53**(20), 8524–8534.
- P. Griefs, *Adv. Cycloaddit.*, 1858, **106**(1), 123–125.
- T. Sandmeyer, *Ber. Dtsch. Chem. Ges.*, 1884, **17**(2), 2650–2653.
- R. Pschorr, *Ber. Dtsch. Chem. Ges.*, 1896, **29**(1), 496–501.
- M. Gomberg and W. E. Bachmann, *J. Am. Chem. Soc.*, 1924, **46**(10), 2339–2343.
- G. Balz and G. Schiemann, *Ber. Dtsch. Chem. Ges.*, 1927, **60**(5), 1186–1190.
- H. Meerwein, E. Büchner and K. van Emster, *J. Prakt. Chem.*, 1939, **152**(7–10), 237–266.
- F. Mo, D. Qiu, L. Zhang and J. Wang, *Chem. Rev.*, 2021, **121**(10), 5741–5829.
- E. Niecke, M. Nieger and F. Reichert, *Angew. Chem., Int. Ed.*, 1988, **27**(12), 1715–1716.
- C. Rømming, P. Karvonen, A. Holm, P. H. Nielsen and J. Munch-Petersen, *Acta Chem. Scand.*, 1963, **17**(5), 1444–1454.
- E. Niecke, R. Detsch, M. Nieger, F. Reichert and W. Schoeller, *Bull. Soc. Chim. Fr.*, 1993, **130**(1), 25–31.
- A. Villinger, P. Mayer and A. Schulz, *Chem. Commun.*, 2006, (11), 1236–1238.
- C. Hu, N. H. Rees, M. Pink and J. M. Goicoechea, *Nat. Chem.*, 2024, **16**(11), 1855–1860.
- X. Wang, Y. Chen, X. Li, L. Xu and G. Tan, *J. Am. Chem. Soc.*, 2025, **147**(41), 36980–36986.
- M. Yoshifuji, I. Shima, N. Inamoto, K. Hirotsu and T. Higuchi, *J. Am. Chem. Soc.*, 1981, **103**(15), 4587–4589.
- D. J. Liptrot and P. P. Power, *Nat. Rev. Chem.*, 2017, **1**(0004), 1–12.
- O. Back, B. Donnadiou, P. Parameswaran, G. Frenking and G. Bertrand, *Nat. Chem.*, 2010, **2**(5), 369–373.
- J. Sun, H. Verplancke, J. I. Schweizer, M. Diefenbach, C. Würtele, M. Otte, I. Tkach, C. Herwig, C. Limberg, S. Demeshko, M. C. Holthausen and S. Schneider, *Chem*, 2021, **7**(7), 1952–1962.
- S. Wang, J. D. Sears, C. E. Moore, A. L. Rheingold, M. L. Neidig and J. S. Figueroa, *Science*, 2022, **375**(6587), 1393–1397.
- Y. Wang, Y. Xie, P. Wei, R. B. King, H. F. Schaefer, P. v. R. Schleyer and G. H. Robinson, *J. Am. Chem. Soc.*, 2008, **130**(45), 14970–14971.
- J. Du, D. Hunger, J. A. Seed, J. D. Cryer, D. M. King, A. J. Wooles, J. van Slageren and S. T. Liddle, *J. Am. Chem. Soc.*, 2021, **143**(14), 5343–5348.
- V. D. Romanenko, *Curr. Org. Chem.*, 2025, **30**, 1–11.
- M. Yoshifuji, *Eur. J. Inorg. Chem.*, 2016, **2016**(5), 607–615.
- D.-L. An, K. Toyota, M. Yasunami and M. Yoshifuji, *J. Organomet. Chem.*, 1996, **508**(1–2), 7–12.
- C. Couret, J. Escudié and J. Satgé, *Tetrahedron Lett.*, 1982, **23**(47), 4941–4942.
- F. Rivière, S. Ito and M. Yoshifuji, *Tetrahedron Lett.*, 2002, **43**(1), 119–121.
- D. Romanenko, V. L. Rudzevich, E. B. Rusanov, A. N. Chernega, A. Senio, J.-M. Sotiropoulos, G. Pfister-Guillouzo and M. Sanchez, *J. Chem. Soc., Chem. Commun.*, 1995, **13**, 1383–1385.
- J. Bresien, C. Hering, A. Schulz and A. Villinger, *Chem.–Eur. J.*, 2014, **20**(39), 12607–12615.
- L. N. Markovskii, V. D. Romanenko, M. I. Povolotskii, A. V. Ruban and E. O. Klebanskii, *Zh. Obshch. Khim.*, 1986, **56**(9), 2157–2158.
- L. N. Markovski, V. D. Romanenko and A. V. Ruban, *Phosphorus, Sulfur Relat. Elem.*, 1987, **30**(1–2), 447–450.
- A. V. Ruban and L. S. Kachkovskaya, *Phosphorus, Sulfur Silicon Relat. Elem.*, 1990, **51**(1–4), 334.



- 40 J. Bresien, K. Faust, A. Schulz and A. Villinger, *Angew. Chem., Int. Ed.*, 2015, **54**(23), 6926–6930.
- 41 J. Bresien, A. Schulz and A. Villinger, *Phosphorus, Sulfur Silicon Relat. Elem.*, 2016, **191**(4), 601–604.
- 42 M. Wu, H. Li, W. Chen, D. Wang, Y. He, L. Xu, S. Ye and G. Tan, *Chem*, 2023, **9**(9), 2573–2584.
- 43 T. Matsuo, K. Suzuki, T. Fukawa, B. Li, M. Ito, Y. Shoji, T. Otani, L. Li, M. Kobayashi, M. Hachiya, Y. Tahara, D. Hashizume, T. Fukunaga, A. Fukazawa, Y. Li, H. Tsuji and K. Tamao, *Bull. Chem. Soc. Jpn.*, 2011, **84**(11), 1178–1191.
- 44 M. Olaru, S. Mebs and J. Beckmann, *Angew. Chem., Int. Ed.*, 2021, **60**(35), 19133–19138.
- 45 Y. He, C. Dai, D. Wang, J. Zhu and G. Tan, *J. Am. Chem. Soc.*, 2022, **144**(11), 5126–5135.
- 46 M. Janssen, S. Mebs and J. Beckmann, *Chem. Commun.*, 2023, **59**(47), 7267–7270.
- 47 M. Wu, W. Chen, D. Wang, Y. Chen, S. Ye and G. Tan, *Natl. Sci. Rev.*, 2023, nwad169.
- 48 M. Janssen, S. Mebs and J. Beckmann, *ChemPlusChem*, 2023, **88**(3), e202200429.
- 49 Y. Chen, M. Wu, D. Wang, N. Yuan, L. Xu and G. Tan, *Organometallics*, 2023, **42**(7), 538–542.
- 50 D. Wang, H. Chen, Y. He, X. Chen, L. Zhang and G. Tan, *Chin. J. Chem.*, 2023, **42**(7), 736–742.
- 51 D. Wang, W. Chen, C. Zhai, L. Zhao, S. Ye and G. Tan, *J. Am. Chem. Soc.*, 2023, **145**(12), 6914–6920.
- 52 D. Wang, C. Zhai, Y. Chen, Y. He, X.-D. Chen, S. Wang, L. Zhao, G. Frenking, X. Wang and G. Tan, *Nat. Chem.*, 2023, **15**(2), 200–205.
- 53 Y. Pang, N. Nöthling, M. Leutzsch, L. Kang, E. Bill, M. van Gastel, E. Reijerse, R. Goddard, L. Wagner, D. SantaLucia, S. DeBeer, F. Neese and J. Cornella, *Science*, 2023, **380**(6649), 1043–1048.
- 54 H. Chen, W. Chen, D. Wang, Y. Chen, Z. Liu, S. Ye, G. Tan and S. Gao, *Angew. Chem., Int. Ed.*, 2024, **63**(20), e202402093.
- 55 M. Janssen, T. Frederichs, M. Olaru, E. Lork, E. Hupf and J. Beckmann, *Science*, 2024, **385**(6706), 318–321.
- 56 Y. Chen, P. Su, D. Wang, Z. Ke and G. Tan, *Nat. Commun.*, 2024, **15**(4579), 1–9.
- 57 X. Li, Y. Zhang, Z. Wang, Z. He, L. Xu and G. Tan, *Organometallics*, 2025, **44**(22), 2620–2624.
- 58 Z. Wang, C. Ding, Y. Chen, M. Huang, D. Wang, L. Xu, S. Pan, S. Ye and G. Tan, *Nat. Chem.*, 2026, **18**(2), 356–363.
- 59 G. Tan and S. Ye, *Acc. Chem. Res.*, 2025, **59**(3), 397–410.
- 60 M. Brynda, *Coord. Chem. Rev.*, 2005, **249**(19–20), 2013–2034.
- 61 J. T. Fleming and L. J. Higham, *Coord. Chem. Rev.*, 2015, **297–298**, 127–145.
- 62 A. A. Nasrullah, M. Fischer, F. Dankert, E. Barath and C. Hering-Junghans, *Organometallics*, 2025, **44**(7), 788–791.
- 63 L. Liu, D. A. Ruiz, D. Munz and G. Bertrand, *Chem*, 2016, **1**(1), 147–153.
- 64 A. H. Cowley, J. E. Kilduff, T. H. Newman and M. Pakulski, *J. Am. Chem. Soc.*, 1982, **104**(21), 5820–5821.
- 65 P. Jutzi, U. Meyer, B. Krebs and M. Dartmann, *Angew. Chem.*, 1986, **98**(10), 894–895.
- 66 R. C. Smith, E. Urnezus, K.-C. Lam, A. L. Rheingold and J. D. Protasiewicz, *Inorg. Chem.*, 2002, **41**(20), 5296–5299.
- 67 A.-M. Caminade, M. Verrier, C. Ades, N. Paillous and M. Koenig, *J. Chem. Soc., Chem. Commun.*, 1984, (13), 875–877.
- 68 R. Deka, M. Temel, S. Crespi and A. Orthaber, *Dalton Trans.*, 2025, **54**(38), 14241–14253.
- 69 A. Hinz, A. Schulz and A. Villinger, *Angew. Chem., Int. Ed.*, 2015, **54**(9), 2776–2779.
- 70 E. Niecke, O. Altmeyer and M. Nieger, *Angew. Chem., Int. Ed.*, 1991, **30**(9), 1136–1138.
- 71 A. H. Cowley, N. C. Norman and M. Pakulski, *J. Chem. Soc., Chem. Commun.*, 1984, **16**, 1054–1055.
- 72 X. Pan, L. Zhang, Y. Zhao, G. Tan, H. Ruan and X. Wang, *Chin. J. Chem.*, 2020, **38**(4), 351–355.
- 73 R. F. W. Bader, *Chem. Rev.*, 1991, **91**, 893–928.
- 74 B. Lindquist-Kleissler, J. S. Wenger and T. C. Johnstone, *Inorg. Chem.*, 2021, **60**(3), 1846–1856.
- 75 (a) CCDC 2501235: Experimental Crystal Structure Determination, 2026, DOI: [10.5517/ccdc.csd.cc2pyr0f](https://doi.org/10.5517/ccdc.csd.cc2pyr0f); (b) CCDC 2501236: Experimental Crystal Structure Determination, 2026, DOI: [10.5517/ccdc.csd.cc2pyr1g](https://doi.org/10.5517/ccdc.csd.cc2pyr1g); (c) CCDC 2501237: Experimental Crystal Structure Determination, 2026, DOI: [10.5517/ccdc.csd.cc2pyr2h](https://doi.org/10.5517/ccdc.csd.cc2pyr2h); (d) CCDC 2501238: Experimental Crystal Structure Determination, 2026, DOI: [10.5517/ccdc.csd.cc2pyr3j](https://doi.org/10.5517/ccdc.csd.cc2pyr3j); (e) CCDC 2501239: Experimental Crystal Structure Determination, 2026, DOI: [10.5517/ccdc.csd.cc2pyr4k](https://doi.org/10.5517/ccdc.csd.cc2pyr4k); (f) CCDC 2501240: Experimental Crystal Structure Determination, 2026, DOI: [10.5517/ccdc.csd.cc2pyr5l](https://doi.org/10.5517/ccdc.csd.cc2pyr5l); (g) CCDC 2501241: Experimental Crystal Structure Determination, 2026, DOI: [10.5517/ccdc.csd.cc2pyr6m](https://doi.org/10.5517/ccdc.csd.cc2pyr6m); (h) CCDC 2512823: Experimental Crystal Structure Determination, 2026, DOI: [10.5517/ccdc.csd.cc2qbrstp](https://doi.org/10.5517/ccdc.csd.cc2qbrstp); (i) CCDC 2512824: Experimental Crystal Structure Determination, 2026, DOI: [10.5517/ccdc.csd.cc2qbsvq](https://doi.org/10.5517/ccdc.csd.cc2qbsvq); (j) CCDC 2523752: Experimental Crystal Structure Determination, 2026, DOI: [10.5517/ccdc.csd.cc2qq5c0](https://doi.org/10.5517/ccdc.csd.cc2qq5c0).

